Monitoring Earth Surface Deformations with InSAR Technology: Principle and Some critical Issues

Yongqi CHEN, Guobao ZHANG, Xiaoli DING and Zhilin LI

Department of Land Surveying & Geo-Informatics
The Hong Kong Polytechnic University
Kowloon, Hong Kong
e-mail: lsyqchen/lszhgb/lsxlding/lszlli@polyu.edu.hk

Abstract

Synthetic aperture radar interferometry, InSAR, is a novel remote sensing technique to measure earth surface deformation. It is capable of obtaining dense information related to the deformation of a large area efficiently, economically and effectively. Therefore, InSAR is a promising technology for monitoring the earth surface deformation related to some natural hazardous events, such as earthquake, volcano eruption, land subsidence, landslide. However, some critical issues need to be addressed before it becomes a reliable and accurate monitoring technology. In this paper, the principles and basic concepts of InSAR are introduced, its applications are reviewed and critical issues on future development examined.

Keywords: Synthetic aperture radar (SAR), InSAR, deformation, remote sensing.

1. Introduction

The deformation of the earth's surface is one of the prominent phenomena associated with many geological hazards, such as landslides, land subsidence, volcano eruption and earthquakes. Earthquake near coastal areas or at sea may in turn cause tsunami (massive tidal waves). Such hazards are severe threats to human life and property. For example, a recent earthquake in Taiwan caused a loss of over 2000 lives and billions of dollars of damage. In July 1998, a tsunami caused by an earthquake with a magnitude 7.0 wreaked havoc across the northwest region of Papua New Guinea, resulting in a loss of 3,000 lives. Such loss and damage would have been avoided or minimised if some kind of warning message could be issued before hand. For any warning system to work effectively, monitoring is essential.

To monitor deformation of earth surface, geotechnical instrumentation, GPS-based systems and many other geodetic techniques are currently available. However, most of them are point-based measurement techniques and are too costly if a very large area needs to be monitored. Recently, a promising alternative area-based technique -- InSAR -- has been explored by researchers, which makes it possible to measure dense points in a study area accurately, economically, conveniently and efficiently [Gabriel et.al., 1989; Massonnet et.al., 1993; Biegert et.al., 1997].

InSAR is the abbreviation of interferometric synthetic aperture radar (SAR). It derives information by using the interferograms, which are formed by phase differences between two complex SAR images of the same area but obtained at slightly different positions with the same sensor or two similar sensors. InSAR can be used to detect the terrain variations

[Zebaker and Goldstein, 1986] and/or deformations [Dixon, 1995]. Under favourable conditions, accuracy at a sub-centimetre level can be reached for deformation measurement, which is good enough for many monitoring purposes. However, some problems associated with the key processing procedures must be tackled before it can become a practically viable measurement technique for deformation monitoring, especially when the gradient of change is significant.

This paper examines some issues on the monitoring of earth surface deformation with InSAR. This introduction is followed by a description of the principles of deformation measurement with InSAR. The application of InSAR in deformation monitoring is reviewed in Section 3 and some critical issues are identified in Section 4. Finally some concluding remarks are made in Section 5.

2. InSAR Technology for deformation measurement: Principles and Concepts

InSAR is based on the use of synthetic aperture radar (SAR). More precisely, it derives information by using the interferograms which are formed by phase differences between two high-resolution complex SAR images of the same area but obtained at slightly different positions. SAR is a microwave imaging radar developed in 1960's to improve the resolution of the traditional (real aperture) radar based on the principle of Doppler frequency shift.

2.1. Principle of the (real aperture) imaging radar

Imaging radar is an active sensor--providing its own illumination in the form of microwaves. It receives and records echo reflected by the target, and then map the intensity of echo into grey scale to form an image. Unlike optical and infrared imaging sensors, such imaging radar is able to take clear pictures day and night under all weather conditions.

Figure 1 shows the geometry of the imaging radar often employed for earth observation. The radar is onboard a flying platform such as an aeroplane or a satellite. It sends microwave to ground continuously with a side-look angle θ in the direction perpendicular to the flying track (azimuth direction). Each time, the energy sent by the imaging radar forms a radar footprint on the ground. This ground area may be regarded as consisting of many small cells. The echo backscattered from each ground cell within the footprint is received and recorded as a pixel in the image plane according to the slant range between the antenna and the ground cell (as shown in Figure 2). During the flying mission, the area swept by the radar footprint forms a swath of the ground, thus a radar image of the swath is obtained.

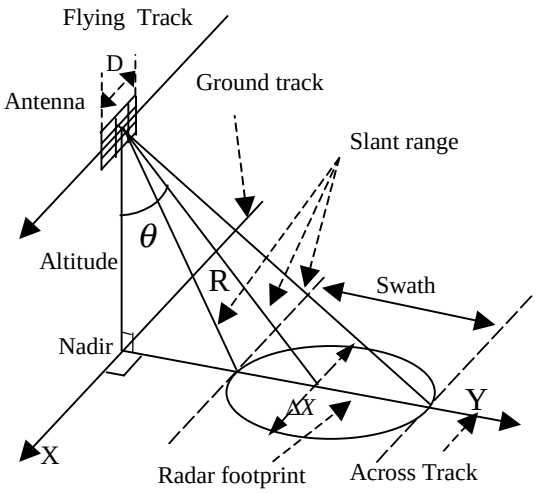

Figure 1 Radar Imaging Geometry

The minimum distance between two distinguishable objects is called resolution of the radar image, which is the most important meausre of radar image quality. Apparently, the smaller this value is, the higher the resolution is. The resolution of a radar image for earth

observation is defined by the azimuth resolution in the flying direction (Δx) and by the slant range resolution in the slant rage direction (ΔR) or the ground range resolution in the cross track direction (Δy), as shown in Figure 3.

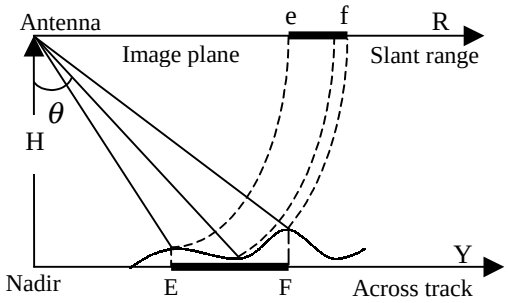

Figure 2 Projection of the radar image

According to the electromagnetic (EM) waves theory, the azimuth resolution is determined by:

$$\Delta x = \frac{R\lambda}{D} \qquad (1)$$

where, R is the slant range, λ is the wavelength of the microwave and D is the length of the aperture of the radar antenna. Here Δx is in fact the width of the footprint as shown in Figure 1. The slant range and ground range resolutions are:

$$\Delta R = \frac{c\tau_p}{2} \qquad (2)$$

$$\Delta y = \frac{c\tau_p}{2\sin\theta} \qquad (3)$$

where, c is the speed of light; τ_p is the pulse duration; and θ is the look angle.

Equations (1)~(3) show that the slant range resolution (or ground range resolution) is characterised only by the property of the microwave and the look angle. They do not have any relationship with the position and size of the antenna. On the other hand, the azimuth resolution (Δx) is dominantly determined by the position and size of the antenna. If a C-band microwave ($\lambda = 5.66cm$) real aperture radar onboard satellite (ERS-1/2) is employed to take images with an azimuth resolution of 10m from 785km away, the length of its aperture is required to be over 3KM. It seems impossible for any flying platform to carry such a long antenna.

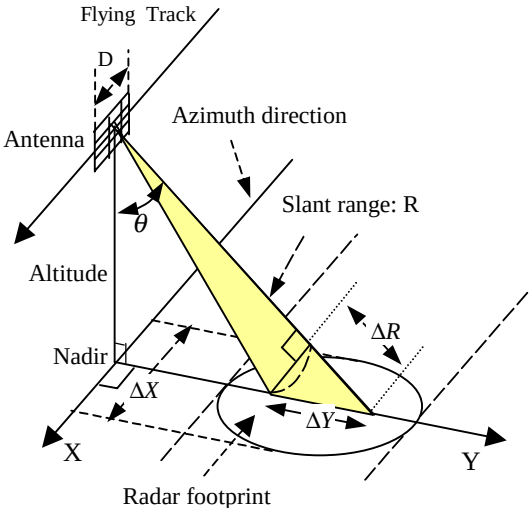

Figure 3 Resolution of the imaging radar

2.2. Principle of the synthetic aperture imaging radar (SAR)

In order to improve the resolution of radar images, synthetic aperture radar (SAR) was developed in 1960s. It is based on the principle of Doppler frequency shift caused by the relative movement between the antenna and the target [Fitch, 1988]. Figure 4 shows the

imaging geometry of synthetic aperture radar while it is being used to take side-looking image of the ground.

Assuming a real aperture imaging radar with aperture length D moves from 'a" to 'b', then to 'c', the slant range from any point, e.g. target O, to the antenna varies from Ra to Rb, then to Rc. It is obvious that Ra > Rb, and Rb <Rc, which means that at first the antenna is flying nearer and nearer to the point object until the slant range becomes the shortest Rb, then it go farther away. The variation of slant range R will cause the frequency shift of the received echo backscattered from point target O, varying from increase to decrease. By precisely measuring the phase delay of the received echoes, tracing its frequency shift, and then synthesising the corresponding echoes, the azimuth resolution can be sharpened, as the area of the intersection of the three footprints shown in Figure 4. Compared with the azimuth resolution of the full footprint width described in the above section, the azimuth resolution (Δx) of synthetic aperture radar (SAR) can be much improved. Ideally,

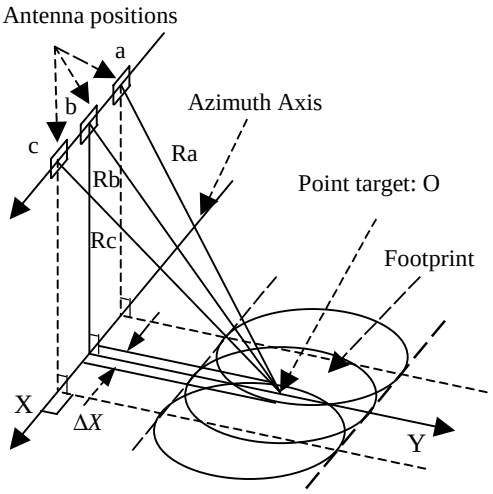

Figure 4 Imaging Geometry of synthetic aperture radar

$$\Delta x = \frac{D}{2} \qquad (4)$$

Indeed, it means that the azimuth resolution (Δx) of a SAR is only determined by the length of the real aperture of an antenna. It becomes independent of the slant range R and the wavelength λ. As a result, it is now possible to acquire images with 10m azimuth resolution by a SAR with real aperture length shorter than 20m onboard ERS-1/2.

Combining with some advanced range compressing techniques, a SAR whether on an aircraft or on a space platform can take high-quality images with high resolution in both azimuth direction X and slant range direction R day and night under all weather conditions, e.g. 4m×8m for ERS-1/2. Figure 5 is an example of SAR image of Yuen Long taken by ERS-2 on March 19, 1996.

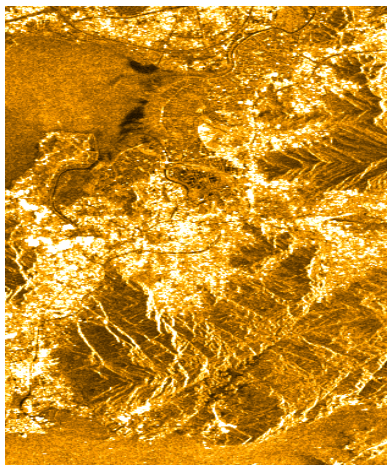

Figure 5 An amplitude SAR image of Yuen Long, Hong Kong, taken by ERS-2 on March 19,1996.

It should be noted here that there is a difference between the traditional real aperture radar and SAR. Coherent microwave is not required by traditional real aperture radar. Images taken by real aperture radar only record the intensity of the echoes. However, microwave sent by a SAR must be coherent in order to measure the Doppler phase shift. The SAR images should

record phase delay as well as the intensity of the echoes. Therefore, a SAR image is generally a complex image containing amplitude component and phase component.

2.3. Basic Principle of Interferometric Synthetic Aperture Radar (InSAR)

SAR images (amplitude image) have been widely used for reconnaissance and environmental monitoring in remote sensing. In such cases, the phase component recorded simultaneously by SAR has been overlooked, indeed for a long time. In 1974, Graham first reported that a pair of SAR images of the same area taken at slightly different positions can be used to form an interferogram and the phase differences recorded in the interferogram can be used to derive topographic map of earth surface [Graham 1974]. Such a technology is called Interferometric SAR (InSAR), or SAR interferometry.

InSAR is a signal processing technique rather than an instrument at present time. It derives information by using the interferogram, $\phi(x,r)$, which records the phase differences between two complex radar images of the same area taken respectively by the same SAR or by two similar SARs from slightly different positions as shown in Figure 6. Let $\hat{S}_1(x,r)$ be the complex images taken at position A1 with its phase component $\Phi_1(x,r)$ and $\hat{S}_2(x,r)$ taken at position A2 with its phase component $\Phi_2(x,r)$. According to radio wave propagation theory, the phase delay measured by an antenna is directly proportional to the slant range from the antenna to a target point.

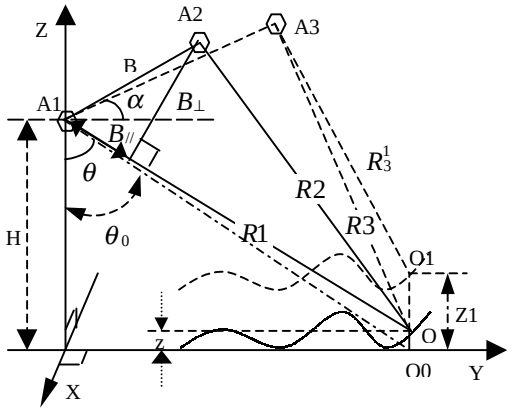

Figure 6 Imaging Geometry of InSAR (or Differential InSAR) for deformation measurement, where R1=R, R2=R+ δR, R3=R+ δ_{R_1}, R_3^1 =R+ δ_{R_1} + δ_{R_2}, Z1=Z+ δZ

$$\Phi = \frac{2\pi R}{\lambda} \tag{5}$$

By subtracting $\Phi_1(x,r)$ from $\Phi_2(x,r)$, the differences form an interferogram $\phi(x,r)$.

$$\phi = \Delta\Phi = \Phi_2 - \Phi_1 = \frac{2\pi Q \delta R}{\lambda} \tag{6}$$

where, $Q=1$, when the two antennas are mounted on the same flying platform, one transmitting wave but both receiving echoes simultaneously to form one-pass interferometry like TOPSAR [Zebker et.al., 1992]; otherwise, $Q=2$.

In order to measure the earth surface deformation of an interesting site within a special interval, it is necessary to take the images of the site with the same SAR or two similar SARs at the starting moment and the end moment of the interval to form repeat-pass InSAR, thus $Q=2$. Parallel flying paths are expected to form repeat-pass InSAR.

From $\phi(x,r)$, the slant range difference (δR) between R1 (the distance from a target point O to A1) and R2 (the distance from O to A2) can be calculated by the following formula:

$$\delta R = \frac{\phi}{4\pi}\lambda \tag{7}$$

where, λ is the wavelength. As λ is in the centimetre order, the slant range difference may be measured in the centimetre order.

If there is no surface change during the interval from A1 to A2, the height Z of the point O can be derived from the following equations:

$$\sin(\theta-\alpha) = \frac{R^2 + B^2 - (R+\delta R)^2}{2RB} \tag{8}$$

$$Z = H - R\cos\theta \tag{9}$$

where, θ is the look angle; B is the length of baseline A1-A2; α is the angle of the baseline with respect to the horizontal line.

If the target point O has moved to position O1 before the antenna moves to position A3, the slant range R3 (denoted by dot line) becomes $R_3^1 = R3 + \delta R_2$, the phase difference (ϕ_{13}^1) between Φ_1 and phase Φ_3 (measured at position A3) is

$$\phi_{13}^1 = \Phi_3 - \Phi_1 = \frac{4\pi}{\lambda}(R_3^1 - R1) = \frac{4\pi}{\lambda}[(R3 - R1) + \delta R_2] = \frac{4\pi}{\lambda}\delta R_1 + \frac{4\pi}{\lambda}\delta R_2 = \phi_{13} + \frac{4\pi}{\lambda}\delta R_2 \tag{10}$$

The first term $\phi_{13} = \frac{4\pi}{\lambda}\delta R_1$ is the topography effect; the second term $\frac{4\pi}{\lambda}\delta R_2$ is the component induced by surface deformation. Given the topography effect, the slant difference δR_2 just induced by deformation is

$$\delta R_2 = \frac{\lambda}{4\pi}(\phi_{13}^1 - \phi_{13}) = \frac{\lambda}{4\pi}\Delta\phi_{13} \tag{11}$$

This equation shows that $\Delta\phi_{13}$ is the difference between two phase difference interferograms. As a result, this technique (to determine the surface deformation) is sometimes called *Differential InSAR* (DInSAR).

After the deformation component in the slant range direction (δR_2) is obtained from Eq.(11), δZ, the height deformation can be caculated easily as follows:

$$\delta Z = Z1 - Z = -\delta R_2 \cos\theta \tag{12}$$

2.4. Three-pass interferometry for deformation measurement

There are two methods to remove topography effects ϕ_{13} from ϕ_{13}^1. One is to use the existing digital elevation model (DEM) of the area to calculate the phase effects of

topography. The other is to use another interferogram as reference so as to form three-pass interferometry [Zebker and Rosen, 1994].

The principle of three-pass interferometry has already been illustrated in Figure 6. In this figure, A1, A2, A3 are succesive positions of the antenna. O is the ground object point, which has not changed during the first time interval (from A1 to A2) but moved to O1 during the interval from A2 to A3. Because $R >> B$, $\delta R \approx B\sin(\theta - \alpha)$, then the difference in the first interferogram

$$\phi \approx \frac{4\pi B\sin(\theta - \alpha)}{\lambda} = \frac{4\pi}{\lambda} B_{//} \qquad (13)$$

where $B_{//} = B\sin(\theta - \alpha)$ is the component of the baseline parallel to the look direction. ϕ here is only related to the topography effects here because there is no variation in the period from A1 to A2. The formula for phase difference in the second interferogram (A1-A3) can then be written as

$$\phi_{13}^{1} \approx \frac{4\pi}{\lambda} B_1\sin(\theta - \alpha_1) + \frac{4\pi}{\lambda}\delta R_2 = \frac{4\pi}{\lambda} B_{1.//} + \frac{4\pi}{\lambda}\delta R_2 \qquad (14)$$

Where α_1 is the angle of the baseline A1-A3 with respect to horizontal line, $B_{1.//} = B_1\sin(\theta - \alpha_1)$ is the component of the baseline parallel to the look direction. By combining (13) and (14), the following can be obtained:

$$\delta R_2 = \frac{\lambda}{4\pi}(\phi_{13}^{1} - \frac{B_{1.//}}{B_{//}}\phi) \qquad (15)$$

This equation shows that slant range deformation δR_2 is determined entirely by the phase differences between the two interferograms, the orbit geometry and the look direction. This means that surface deformation can be measured by three-pass InSAR without prior knowledge of the terrain variation.

The ratio $B_{1.//} / B_{//}$ in equation (15) is a function of look angle θ which is a function of the position of the target point. Mathematically,

$$\frac{B_{1.//}}{B_{//}} = \frac{B_1\sin(\theta - \alpha_1)}{B\sin(\theta - \alpha)} \qquad (16)$$

Generally speaking, it is very difficult to determine angle θ directly without information about terrain variation. Therefore, alternative solutions for δR_2 should be investigated.

If the target point O is at position O_0 where Z=0, as illustrated in Figure 6, the look angle θ_0 can be estimated easily from the position of O_0. Then the phase difference of the two interferograms at point O_0 is

$$\phi_0 \approx \frac{4\pi}{\lambda} B\sin(\theta_0 - \alpha), \quad \phi_{0.13} \approx \frac{4\pi}{\lambda} B_1\sin(\theta_0 - \alpha_1) \qquad (17)$$

Let $\theta = \theta_0 + \delta\theta$. The look angle difference $\delta\theta$ is small. Then,

$$\begin{aligned}\phi_{0.12} &= \phi - \phi_0 \approx \frac{4\pi B}{\lambda}\sin(\theta-\alpha) - \frac{4\pi B}{\lambda}\sin(\theta_0-\alpha) \\ &\approx \frac{4\pi\delta\theta}{\lambda} B\cos(\theta_0-\alpha) = \frac{4\pi\delta\theta}{\lambda} B_\perp\end{aligned} \tag{18}$$

and

$$\begin{aligned}\phi^1_{0.13} &= \phi^1_{13} - \phi_{0.13} \approx \frac{4\pi}{\lambda}\delta R_2 + \frac{4\pi B_1}{\lambda}\sin(\theta-\alpha_1) - \frac{4\pi B_1}{\lambda}\sin(\theta_0-\alpha_1) \\ &\approx \frac{4\pi}{\lambda}\delta R_2 + \frac{4\pi\delta\theta B_1}{\lambda}\cos(\theta_0-\alpha_1) = \frac{4\pi}{\lambda} B_{1.\perp}\delta\theta + \frac{4\pi}{\lambda}\delta R_2\end{aligned} \tag{19}$$

Where, $B_\perp$ and $B_{1.\perp}$ are the vertical component of the two baselines to look direction and are determined by Equations (20) and (21) respectively; $\phi_{0.12}$ and $\phi^1_{0.13}$ are the interferogram phase corrected with horizontal plane effects.

$$B_\perp = B\cos(\theta_0-\alpha) \approx B\cos(\theta-\alpha) \tag{20}$$

$$B_{1.\perp} = B_1\cos(\theta_0-\alpha_1) \approx B_1\cos(\theta-\alpha_1) \tag{21}$$

By combining (18) and (19), one could get

$$\delta R_2 = \frac{\lambda}{4\pi}(\phi^1_{0.13} - \frac{B_{1.\perp}}{B_\perp}\phi_{0.12}) \tag{22}$$

This equation shows that the surface deformation can be measured without any knowledge of the terrain information with three-pass InSAR.

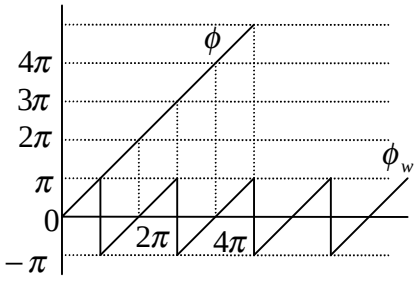

Figure 7 Phase and unwrapped phase

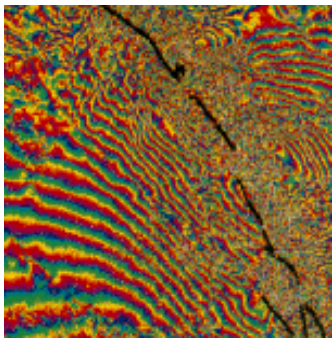

Figure 8 A section of coseismic interferograms for Landers earthquake.

It should be pointed out that the phase in the above equations can vary from $-\infty$ to $+\infty$, but the actual value measured by SAR has been wrapped into $(-\pi,\pi)$. The relationship between wrapped ϕ_w and its original value ϕ is shown in Figure 7 and can be expressed as:

$$\phi = \phi_w + 2k\pi \tag{23}$$

Where, $\phi_w \in (-\pi,\pi)$, k is an integer. An inteferogram generated by InSAR is, in fact, an image of the wrapped phases and thus variation of the phase value often forms fringes in the interferogram as shown in Figure 8. In order to use the above equations to obtain

information about the deformation of the earth surface, the wrapped phase should be unwrapped into its original phase with a process called “phase unwrapping”, which is a critical problem in InSAR [Ghiglia and Pritt, 1998].

3. Application of InSAR in earth surface Deformation Studies

SAR systems can be either airborne or spaceborne. For deformation monitoring, the latter is more widely used. This is because repeat-pass or multi-pass InSAR is required to measure the earth surface deformation but aircraft is not able to fly sufficiently close to its previous path and therefore it is very difficult to form repeat-pass or multi-pass airborne InSAR. As a result, emphasis in this section will be on the applications of spaceborne InSAR in deformation monitoring.

3.1. Monitoring earthquake

Earthquakes are always related to crustal deformation of a large area. Measuring or monitoring the deformation of a seismic area is a means to acquire critical information for understanding and even forecasting earthquakes.

The first result on this topic was reported by Massonnet et.al. [1993]. This was about the deformation caused by a large earthquake with magnitude 7.3 struck near the town Landers in southern California on 28 June 1992. In their study, four ERS-1 SAR images taken on 12 April, 3 July, 7 August and 11 September of 1992 were used to form three interferograms of the desert area with a size of 113 km by 90 km. The interferogram generated from the April 24 and August 7 (with 105-day interval) was used to derive the slant range displacements related to the earthquake as this interferogram was found to be of the best coherence. A differential interferogram is then formed after removing the topography effects from the interferogram by use of a DEM of the area. This differential interferogram consists of a set of fringes as shown in Figure 8. One circle of fringe represents a slant range difference of 28mm. Accuracy was assessed by comparing the results obtained with traditional geodetic methods. A RMS of about 34mm was found in the coherent area. On the other hand, if the coherence is not good enough, the method will fail. The black area in Figure 2-2 shows the case. In this area, there is a fault strip of 5-10 km long with displacement of 4m ~ 6m. No deformation information could be obtained in this area by InSAR technology.

Similar measurement results were also reported by Zebker and Rosen [1994]. But in their case, no DEM (digital elevation model) is used to remove topographic effects. Two pairs of ERS-1 SAR images were selected to form two interferograms. One is the April/August pair and the other is the July/August pair. The first pair spans the earthquake on June 28. As a consequence, the interferogram contains information about both topographic effects and phase differences induced with surface deformation. The second pair was taken after the earthquake. Therefore, the interferogram formed from this second pair includes only the information about topographic effects. Coseismic displacement in the slant range direction is then derived from the differential interferogram. A mean value of the differences is 0.9cm and corresponding RMS is 18.9 cm in the coherent area as compared with the results obtained with GPS and EDM.

Other researchers have also reported the measurement of deformations caused by earthquakes [Fujiwara and Rosen, 1998; Stramondo et.al., 1999]. All these experiments demonstrate that InSAR is a promising tool to measure the earth surface deformations related to earthquake with required precision.

3.2. Monitoring Volcano

The earth surface deformation is also an important characteristic related to volcano activities. There are a series of deformations around a volcano characterized by inflation before its eruption and deflation afterward. Monitoring such deformations has also been carried out by means of InSAR.

The first report was on the observation of the Mount Etna volcano in the island of Sicily (Italy). The volcano is one of the most active and the best-studied volcanoes in the world. The most recent eruption started on 14 December 1991 and ended on 31 March 1993. It lasted for 473 days. Massonnet et al [1995] used two families of ERS-1 SAR images, which were taken from 17 May 1992 to 24 October 1993, to form about 30 interferograms to detect the crustal deformation around the volcano. After removing terrain effects with a given EDM, a series of interferograms which represented the deformation around the volcano was obtained. Figure 9 shows a part of such an interferogram, where each contour line represents 28mm (i.e. half of the wavelength). From the set of interferograms, a deflation model of the volcano during the eruption with the accuracy of 1cm was built.

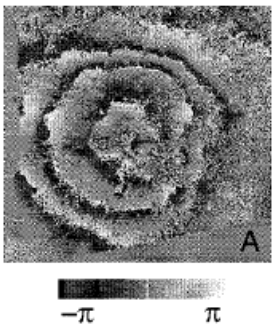

Figure 9 A section of differential interferograms, 92/9/27-93/10/17.

For the same volcano, Sansosti *at al*., (1998) used 19 interferograms of the area taken by ERS1/2 from 1992 to 1996 to monitor the deformation related to its activity. After removing the topography effects with a DEM, information about the deformation was obtained from the interferograms by removing topographic effect using a DEM. It was found that the 1992-1993 interferograms indicate a strong subsidence signal during the eruptive period but the trend had been reversed since 1993. The interferograms spanning 1993-1995 indicate a strong inflation signal, while the interferograms from 10 October 1995 to 30 October 1996 indicate small deformations in this area. Such a deformation model was in accordance with results observed by GPS.

Some recent work on measuring the deformation of the volcano by InSAR has been reviewed by Wadge [1997]. Examples are volcano eruption on 30 September 1996 in the Vatanjokull Glacier in Iceland [Thiel *et.al*., 1997] and the flank eruption of Fernandia volcano in Galapagos in Ecuador in 1995 [Jonsson, *et.al*., 1999].

3.3. Monitoring Land Subsidence

Land subsidence is a worldwide phenomenon. It may result from many factors, such as tectonic movements, stretching of lithosphere, underground mining, heavy withdraw of groundwater, and so on. Land subsidence usually develops slowly but it may result in serious problems or hazards. For example, serious land subsidence can affect or damage the ability to extract miming exploitations. Monitoring such phenomena continuously is an important procedure for forecasting or preventing hazards

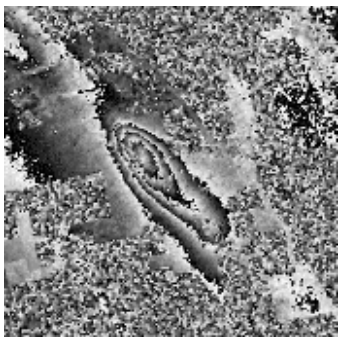

Figure 10 A section of the differential interferogram of the deformation of the Belridge oil field between 104 days.

caused by land subsidence. InSAR has also been used for such monitoring as conventional geodetic techniques are only feasible for measurement at sparse points [Halsema and Kooij, 1996].

Kooij [1997] tried to observe land subsidence due to oil and gas exploitation at the Belridge and Lost Hills Oil Fields. The oil fields are located approximately 100 km West of Bakersfield (U.S.A.) with an area of approximately 20 by 5 km. Land subsidence at the field costs millions of dollars per year, and sometimes stops the oil production temporarily. In this study, multiple interferograms obtained from ERS-1/2 during 1995-1996 were used. An interferogram was first selected to estimate a reference DEM, then it was used as reference to remove the terrain effects for other interferograms to acquire differential interferograms corresponding to height change. The accuracy was in the order of centimeters at the oil field spanning different periods. Figure 10 shows a section of the differential interferogram created from ERS data (ERS-1 February 17, 1996 and ERS-2, April 28, 1996). In this Figure, each fringe indicates slant changes of 28mm. In the same field, Biegert *et al.*, [1997] obtained similar results using data set from RADARSA.

Halsema and Kooji [1996] measured land subsidence related to gas exploitation in Zeeland and Groningen areas in Netherlands. In their study, 30 interferograms were generated from 50 ERS-1 images obtained during a period of 2 to 3 years. Wright and Stow measured mining subsidence of the Selby Coalfield in the UK and the Silesain Coalfield in Czech Republic [Wright and Stow, 1997]. In their study, images from ERS-1/2 were used to form interferograms. Amelung et al. detectd the land subsidence related to persistent overdraft of groundwater in Las Vegas [Amelung *et al*., 1999]. They used interferograms of ERS-1/2 from April 1992 to December 1997.

3.4. Monitoring Landslide

InSAR has also been used for monitoring landslide although the sliding areas are generally quite small and often with high topography, which make the task more difficult. Fruneau et al. tried to employ InSAR to monitor the deformations of the “La Clapiere” landslide which is located near Nice, in Southern France, on the left bank of Tinee River [Fruneau et al., 1996]. The “La Clapiere” landslide extends over a few square kilometers with height variation between 1100m and 1700m. ERS-1 SAR images taken in 1991 were used to form a set of differential interferograms of the area. It was found that the earth surface deformation related to landslide was really reflected in such kind of differential interferograms.

Singhroy and his colleagues [Singhroy et. al., 1998] did similar experiments at the Fraser valley, Saskatchewan and Ottawa River valley in Canada. It was found that interferograms generated from RADARSAT SAR images could be used to identify diagnostic features of landslides and slope characteristics.

4. Some Critical Issues with Current InSAR Technology

As has been discussed in the previous section, experiments with InSAR have been carried out for measurement of deformations caused by some natural phenomena. It has been demonstrated that InSAR is a promising technology for this purpose. However, InSAR is not a perfect technology. It needs improvement in a number of aspects. In another word, there are some problems yet to be solved. Some of these issues are discussed in this section.

4.1. Accuracy of image co-registration

Images must be first registered in order to generate an interferogram. In this process, two pixels of the same point target from two different SAR images are matched. Mis-registration is a common problem. Such mis-registration, even on sub-pixel basis, may result in serious errors or coherence loss [Fornaro and Franceschetti, 1995].

Mis-registration is related to the recorded amplitude and phase values of individual pixels, which are results of coherent interference of back-scattered radio microwaves from a number of back-scattering targets. Mis-registered pixels represents slightly different scattering targets and different interference patterns, as shown in Figure 10. In practice, it is very difficult to get accurate registration due to overlap and foreshortening.

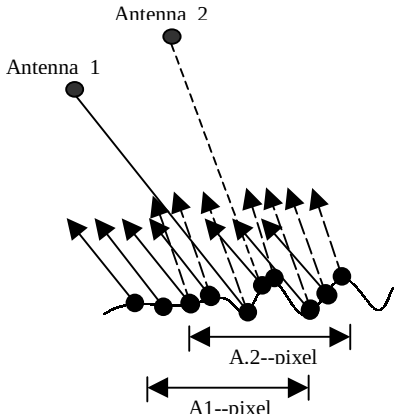

Figure 10 Misregistered pixels

Current registration algorithms are usually based on the evaluation of a merit function, such as the correlation function [Li and Goldstein, 1990], the signal to noise ratio (SNR) [Gabriel and Goldstein, 1988] or average fluctuation [Lin et.al., 1992]. The registration is determined when the merit function reaches its optimum value through the calculation of different offsets. Theoretically speaking accuracy of sub-pixel level can be reached in the registration. For example, Li and Goldstein [1990] reported an accuracy of 0.05 pixel. Such a figure seems very small. However, it may cause a complete loss of coherence in the areas with high relief and/or with abrupt changes.

4.2. Accuracy of baseline estimation

Baseline plays a very important role in the measurement of the earth surface deformation with InSAR. An accuracy of centimetre is required for baseline length and its components. However, current orbit parameters provided with SAR images cannot satisfy this requirement. As a consequence, it is necessary to develop effective methods to estimate accurate baseline parameters [Seymour and Cumming, 1996].

There are four different approaches to estimate the precise baseline parameters for current InSAR systems, i.e.

a) To estimate the parameters based on the interferometric fringes appearing in flat areas as the fringes are only related to baseline altitude;
b) To determine the baseline based on more than three interferometric sets of the same site [Kimura, 1995];
c) To calculate the orbit based on more than 7 ground control points (GCP) [Kimura and Todo, 1997]; and
d) To fit the satellite orbit based on given satellite orbit state vectors [Rufino and Moccia, 1996].

For the first approach, it is very difficulty to find a really flat area. For the second, the baseline accuracy cannot be assured in the optimization process. For the third approach, it is often the case that there are not enough precise ground control points in the area corresponding to the interferogram although this approach is often employed practically.

The fourth approach is often employed to estimate the baseline of ERS-1/2 because there are plenty of quite precise orbit data provided, but not for JERS-1 or RADARSAT.

Indeed, these approaches can solve the problem to some extent. However, the inaccuracy of the estimated baseline parameters is still a main error source in the measurement of the earth surface deformation. It has been realized that to design a new interferometry device binding with precision position determiner, i.e. GPS, is the best way to solve the problem [Malliot, 1996].

4.3. Reliability of phase unwrapping algorithm

As pointed out previously, phase unwrapping is a very important and difficult problem with InSAR. To design an algorithm to restore accurate phase value from the wrapped value has been a hot topic for a long time. Most of the current phase unwrapping algorithms include two steps: estimation of the unwrapped phase gradient and integration along a path connecting the image pixel [Fornaro et.al., 1996]. It is, however, very difficult to decide a proper path for integration. As a consequence, the result is very sensitive to noises (see next sub-section) because such algorithms may result in drastic error propagation.

A type of optimum algorithms, mainly based on least squares method, has been put forward in order to reduce the error propagation [Reigber and Moreira, 1997], but it may not restore the real phase and often fails in low coherence areas. Another algorithm, region-growing algorithm, has been put forward recently [Xu and Cumming, 1999]. It reduces the level of error accumulation in the integration process to some extent by selecting the optimal integration path. It works in areas with some lower coherence. However, computation load will be increased dramatically while there is no guarantee of improvement in accuracy of the unwrapped values. Therefore, development of a robust and accurate phase unwrapping algorithm is a matter of some urgency.

4.4. Noise from various sources

The three issues addressed in previous sub-section, i.e. image co-registration, baseline accuracy and phase unwrapping are indeed the three key procedures in signal processing in an InSAR system. Another issue will be the noise coming from various sources such as *the faults of signal processing procedure*, atmospheric effects, baseline decorrelation and temporal decorrelation. Such noises have to be treated carefully in order to get accurate measurement.

Although a SAR is advantageous in taking high-quality radar images under all weather conditions, phase delay due to the difference of weather conditions may cause serious errors in InSAR measurement. When microwave is propagating through the media of atmosphere, it may result in excessive phase delays, namely the atmospheric effects, especially in rich water vapor area or on raining days. Atmospheric heterogeneity at different times may cause serious phase errors or even coherence loss for repeat-pass or multi-pass interferometry. Atmospheric effects vary with pressure, temperature, relative humidity and other atmospheric parameters. It is almost impossible

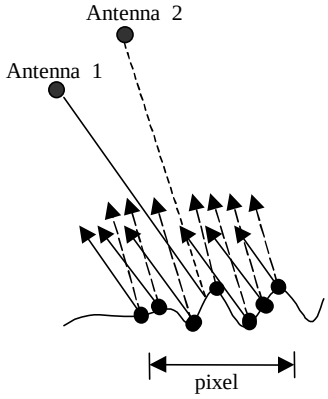

Figure 11 Baseline decorrelation

to set up a robust mathematical model to estimate its quantity [Hanssen and Feijt, 1996]. Therefore, in most InSAR experiments, arid areas are often selected as test sites since the phase errors due to atmospheric effects in the arid areas can almost be neglected. However, if one really wants to leave laboratory to make InSAR a practical technology to monitor the earth surface deformation, the problem of atmospheric effects must be tackled.

Baseline decorrelation is another error source. A SAR image cell can be regarded as a record of echoes from a set of distributed scattering targets, as illustrated in Figure 11. Echoes from these targets may produce random coherent interference. When a specific pixel is imaged from a slightly different viewing geometry, a different interference pattern will be generated. Therefore, for the same pixel in different images taken at different positions such as Antenna 1 and Antenna 2, they may result in different phase and/or amplitude values. As these differences are due to the difference in antenna's viewing geometry, this phenomenon is called baseline decorrelation. This decorrelation may cause a decrease or even loss in coherence between SAR images. Therefore, it should also be carefully dealt with [Franceschetti et.al., 1996; Zebker and Villasenor, 1992]. It is obvious from Figure 11 that baseline decorrelation will increase with an increase in the baseline vertical component $B_\perp$ and decrease with a decrease in $B_\perp$. It is also true that the shorter the baseline $B_\perp$, the lower degree of baseline decorrelation is. However, a shorter baseline $B_\perp$ will reduce the measurement sensitivity. Therefore, there should be a trade-off to select baseline.

Temporal decorrelation refers to the decorrelation between two images taken at different epochs. It may be caused by the variations of many factors with time, such as atmospheric heterogeneity, vegetation, change in soil properties, and earth surface change. It might be the most significant noise source in repeat-pass or multi-pass interferometry employed in the deformation measurement with current InSAR [Zebker and Villasenor, 1992; Villasenor and Zebker, 1992]. Current methods try to fuse multiband interferograms or multi baseline interferograms to obtain more robust results. However, fusion of different interferograms is also a very difficult problem. Therefore, so far, there is a lack of effective method to treat temporal decorrelation.

4.5. Limitation in data sources

As pointed out previously, airborne SAR is not suitable for the formation of repeat-pass or multi-pass InSAR for monitoring the earth surface deformation. In another word, only images taken by spaceborne SARs can be used for the purpose. In fact, only SARs on satellites can be taken as the stable data sources to provide the required SAR images for civil usage because space shuttle missions are not regularly scheduled. Satellite SAR includes European ERS-1 and ERS-2, Japanese JERS-1, Canadian RADARSAT, and JPL SEASAT (Table 1). Among them, only ERS-1, ERS-2, and RADARSAT are still in operation and may be used to monitor earth surface deformation at present or in near future.

Although it has been claimed that these spaceborne SAR systems are able to take images of any place of the earth, there is no guarantee that images of the same area taken at different times would have sufficient level of coherence to form repeat-pass interferometric sets. Among those available SAR images, only a small portion can, in fact, be used to form repeat-pass interferograms at present due to the baseline and temporal decorrlation problems. Lack of enough interferometric sets has become a serious problem to prevent InSAR from being a practical measurement tool at current stage.

5. Concluding Remarks

In this paper, the principle of the earth surface deformation measurement with InSAR has first of all been introduced; its applications in monitoring the deformation due to earthquake, volcano eruption, land subsidence, and landslide are then outlined; some critical issues on InSAR technology as a deformation monitoring technology are also addressed.

In fact, the application of InSAR is not limited to those described in this paper. Indeed, it has also tested in monitoring of flood [Geudtner et.al., 1996], detection of ice movement [Mattar et.al., 1998], as well as monitoring of crustal deformation related to large areas.

Table 1: Current available spaceborne SAR systems

Mission	ERS-1	ERS-2	JERS-1	RADARSAT	SEASAT
Owner	The European Space Agency	The European Space Agency	Japan	Canadian Space Agency	JPL
Launch Date	July 16, 1991	20 Apr. 1995	Feb. 11, 1992	Nov. 4, 1995	June 27, 1978
Ended Date			12 Oct. 1998		Oct. 10, 1978
Band	C (5.7 cm, 5.25 GHz)	C (5.7 cm, 5.25 GHz)	L (23.5 cm, 1.275 GHz)	C (5.7 cm, 5.3 GHz)	L (23.5 cm, 1.275 GHz)
Polarization	VV	VV	HH	HH	HH
Look angle	20-26	20-26	35º(38º)	20-50	20º (23º)
Swath	100 km	100 km	75 km	45-500 km	100 km
Range Resolution	20 m	20 m	18 m	10-100 m	25 m
Azimuth Resolution	30 m	30 m	18 m	10-100 m	25 m
Left/Right Looking	right	right	right (yaw 180º to map Antarctica)	right or (two 2-week periods of left-looking to map Antarctica	
Looks	4	4	3	1-16	4
Orbit	Altitude: 785km and an inclination of 98.5 degrees (known as the reference orbit).	Altitude : 785 km and an inclination of 98.5 degrees (known as the reference orbit).	Altitude : 568 km, inclination:98 degree	Altitude: 798 km, inclination of 98.6 degrees.	Altitude: 800 km (500 miles) in a nearly circular, near-polar orbit

In the recent years, some InSAR signal processing software packets, i.e. EvInSAR [Kooij et.al., 1996], CivInSAR [Haynes et.al., 1997] and other products [Gens, 1998], have been developed and tested in the measurement of the deformation. However, there are still some critical issues to be addressed before it becomes a practically useful. These issues include improvement in accuracy of image co-registration, baseline estimation and phase unwrapping as well as reduction of noise effects. These issues are mainly due to the fact that current spaceborne SAR systems are originally designed for high-resolution amplitude

radar images rather than for interferometry. Some good ideals on future SAR systems for interferometry have been put forward such as tethered InSAR [Moccia and Vetrella, 1992], three antennas on a platform [Corsini et.al., 1997] and binding GPS device with antenna [Malliot, 1996]. It is the opinion of the authors that InSAR may be enhanced in two directions. Firstly, efforts are to be made to improve current InSAR technique so as to make it more robust and reliable. Alternatically, special spaceborne SAR systems for InSAR might be considered.

In conclusion, InSAR has recently attracted more and more attention in the field of monitoring the earth surface deformation because it has many advantages over the other survey techniques (Biegert at al., 1997). Realistically speaking, InSAR is currently not the most accurate measurement technology, but it is certainly one of the most promising one. On the other hand, at present, InSAR is the only technology to monitor the deformation of the earth surface in a large area with dense points, accurately, quickly and cost-effectively in day and night under all weather conditions, although there are still a lot of improvement to be made. It is confident to state that, with the development of this technology, an effective and economical system for the monitoring of earth surface deformation may be set up by using InSAR as its backbone.

Acknowledgement

The work described in this paper forms part of the AOE project and a research project with number G.34.37.T022, both of which are supported by the Hong Kong Polytechnic University.

References

Amelung, F., Galloway, D.L. and Zebker, H.A., (1999). Sensing the ups and downs of Las Vegas: InSAR reveals structural control of land subsidence and aquifer-system deformation. *Geology*, Vol. 27, No. 6, pp.483—486.

Biegert, E.K., Berry, J.L. and Oakley, S.D., (1997). Oil field subsidence monitoring using spaceborne Interferometric SAR: a Belridge 4-D case history. Atlantis Scientific Inc., *http://www.atlsci.com/library/papers/Oil_field_Subsidence_Monitoring_using_Spaceborne_Interferometric_SAR.html* , 1997.

Corsini, G., Diani, M., Lombardini, F. and Pinelli, G., (1997). Reduction of the phase-unwrapping drawbacks by the three-antenna interferometric SAR system. *IGARSS '97 - 1997 IEEE International Geoscience and Remote Sensing: Remote Sensing - A Scientific Vision for Sustainable Development*, Vol.4, pp.1536–1538.

Dixon, T. H., (1995). SAR interferometry and surface change detection. *Report of a workshop on the scientific applications and technical challenges of a new technique for remotely monitoring the Earth's surface from space.* Boulder, Colorado. February 3-4, 1994. Updated: Sept. 1995. http://southport.jpl.nasa.gov/scienceapps/dixon/index.html.

Doyle, G.S., Inggs, M.R. and Hartnady, C.J.H., (1997). The use of interferometric SAR in a study of reservoir induced crustal deformation. *COMSIG '97 - Proceedings of the 1997 South African Symposium on Communications and Signal Processing*, pp.5–8.

Fitch, J.K., (1988). *Synthetic aperture radar*. Springer-Verlag, Berlin, Germany, 1988.

Fornaro, G. and Franceschetti, G., (1995). Image registration in interferometric SAR processing. *IEE Proceedings - Radar, Sonar and Navigation*, Vol.142, No.6, pp.313 – 320.

Fornaro, G., Franceschetti, G. and Lanari, R., (1996). Interferometric SAR phase unwrapping using Green's formulation. *IEEE Transactions on Geoscience and Remote Sensing*, Vol. 34, No.3, pp.720 –727.

Franceschetti, G., Iodice, A., Migliaccio, M. and Riccio, D., (1996). On the baseline decorrelation. *IGARSS '96 - 1996 International Geoscience and Remote Sensing Symposium on 'Remote Sensing for a Sustainable Future'*, Vol.1, pp.680 –682.

Fruneau, B., Delacourt, C. and Achache, J., (1996). Observation and modeling of the Saint-Etienne-de-Tinée landslide using SAR interferometry. *FRINGE'96 - ESA Workshop on Applications of ERS SAR Interferometry, Zurich, Switzerland, 30 September to 2 October 1996*. http://www.geo.unizh.ch/rsl/fringe96/papers/fruneau/.

Fujiwara, S. and Rosen, P.A., (1998). Crustal deformation measurements using repeat-pass JERS-1 sythetic radar interferometry near the Izu Peninsula, Japan. *Journal of Geophysical Research*, Vol. 103, No. B2, pp.2411-2426.

Gabriel, A.K. and Goldstein, R.M., (1988). Crossed orbit interferometry: theory and experimental results from SIR-B. *International Journal of Remote Sensing*, Vol.9, No.5, pp.857-872.

Gabriel, A.K., Goldstein R.M. and Zebaker H.A., (1989). Mapping small elevation changes over large areas: differential radar interferometry. *Journal of Geophysical Research*, Vol.94, No.B7, pp.83-91.

Gens, R., (1998). *Quality assessment of SAR interferometric data*. Doctoral Dissertation, University of Hannover, Germany, pp.121-138.

Geudtner, D., Winter, R. and Vachon, P. W., (1996). Flood monitoring using ERS-1 SAR interferometry coherence maps. *IGARSS '96 - 1996 International Geoscience and Remote Sensing Symposium on Remote Sensing for a Sustainable Future*, Vol.2, pp.966–968.

Geudtner, D., Vachon, P. W., Matter, K.E. and Gray, A.L., (1998). RADARSAT repeat-pass SAR interferometry. *IGARSS'98 - Proceedings of the1998 IEEE International Geoscience and Remote Sensing Symposium*, Vol. 3, pp.1635-1637.

Ghiglia, D.C. and Pritt, M.D., (1998). *Two-dimensional phase unwrapping: theory, algorithms, and software*. John Wiley & Sons, INC., U.S.A., 1998.

Graham, L.C., (1974). Synthetic Interferometric radar for topographic mapping. *Proceedings of IEEE*, vol.62, pp. 763-768.

van Halsema, D. and van der Kooij, M.W.A, (1996). Satellite radar measurements of land subsidence. *IGARSS '96 - 1996 International Geoscience and Remote Sensing Symposium on Remote Sensing for a Sustainable Future*, Vol. 2, pp. 963 –965.

Hanssen, R. and Feijt, A., (1996). A first quantitative evaluation of atmospheric effects on SAR interferometry. *FRINGE'96 - ESA Workshop on Applications of ERS SAR Interferometry, Zurich, Switzerland, 30 September to 2 October 1996*. http://www.geo.unizh.ch/rsl/fringe96/papers/hanssen/.

Haynes M, Capes R., Lawrences G., Smith A., Shilston D. and Nicholls G., (1997). Major urban subsidence mapped by differential SAR Interferometry. *The 3rd ERS Symposium (ESA), Florence, Italy. March 18-21, 1997*. http://www.npagroup.co.hk/html/civinsar/florence.html.

Jonsson, S., Zebker, H., Cervelli, P. and Segall, P., (1999). A shallow-dipping dike fed the 1995 flank eruption at Fernandia Volcano, Galapagos, observed by satellite radar interferometry. *Geophysical Research Letters*, Vol. 26, No. 8, pp.1077-1080.

Kimura, H., (1995). A method to estimate baseline and platform altitude for SAR interferometry. *IGARSS '95 - 1995 International Geoscience and Remote Sensing Symposium on Quantitative Remote Sensing for Science and Applications*, Vol.1, pp.199 -201.

Kimura, H. and Todo, M., (1997). Baseline estimation using ground points for interferometric SAR. *IGARSS '97 - 1997 IEEE International Geoscience and Remote Sensing, Remote Sensing - A Scientific Vision for Sustainable Development*, Vol.1, pp.442 -444.

van der Kooij, M.W.A., Armour, B., Ehrismann, J., Schwichow, H. and Sato, S., (1996). A workstation for spaceborne interferometric SAR Data. *IGARSS'96 - 1996 International Geoscience and Remote Sensing Symposium on Remote Sensing for a Sustainable Future*, Vol.1, No.1, pp.339 -341.

van der Kooij, M., (1997). Land subsidence measurements at the Berlridge Oil Fields from ERS InSAR data. *Atlantis Scientific Inc*., http://www.atlsci.com/library/papers/.

Li, F.K. and Goldstein, R.M., (1990). Studies of multibaseline spaceborne interferometric synthetic aperture radars, *IEEE Transaction on Geoscience and Remote Sensin*g, Vol.28, No.1, pp.88-97.

Lin, Q., Vesecky, J.F. and Zebker, H.A, (1992). Registration of interferometric SAR images. *IGARSS '92 - 1992 International Geoscience and Remote Sensing Symposium*, Vol.2, pp.1579 –1581.

Malliot, H.A, (1996). DTEMS interferometric SAR design and method of baseline tilt determination. *Proceedings of 1996 IEEE Aerospace Applications Conference*, Vol.4, pp.107 –127.

Massonnet, D., Rossi, M., Carmona, C., Adragna, F., Peltzer, G., Feigl K. and T. Rabaute, (1993). The displacement field of the Landers Earthquake mapped by radar interferometry. *Nature*, Vol. 364, pp. 138-142.

Massonnet, D., Briole P. and Armaud, A., (1995). Deflation of Mount Etna monitored by spaceborne radar interferometry. *Nature*, Vol.375, pp.567-570.

Mattar, K.E., Vachon, P.W., Geudtner, D., Gray, A.L., Cumming, I.G. and Brugman, M., (1998). Validation of Alpine glacier velocity measurements using ERS tandem-mission SAR data. *IEEE Transactions on Geoscience and Remote Sensing*, Vol.36, No.3, pp.974 -984.

Moccia, A. and Vetrella, S., (1992). A tethered interferometric synthetic aperture radar (SAR) for a topographic mission. *IEEE Transactions on Geoscience and Remote Sensing*, Vol.30, No.1, pp.103 –109.

Reigber, A. and Moreira, J., (1997). Phase unwrapping by fusion of local and global methods. *IGARSS '97 - 1997 IEEE International Geoscience and Remote Sensing: Remote Sensing - A Scientific Vision for Sustainable Development*, Vol.2, pp.869 –871.

Rufino, G. and Moccia, A., (1996). ERS orbit and attitude modelling for interferometric applications. *The 3rd ERS Symposium (ESA), Florence, Italy. March 18-21, 1997.* http://florence97.ers-symposium.org/papers/participants/data/rufino/.

Sansosti, E., Lanari, R. and Lundgren, P., (1998). Dynamic deformation of Etna volcano observed by satellite radar interferometry. *IGARSS '98 - 1998 IEEE International Geoscience and Remote Sensing Symposium Proceedings*, Vol. 3, pp.1370 -1372.

Seymour, M.S. and Cumming, I.G., (1996). An iterative algorithm for ERS baseline estimation. *FRINGE'96 - ESA Workshop on Applications of ERS SAR Interferometry, Zurich, Switzerland, 30 September to 2 October 1996.* http://www.geo.unizh.ch/rsl/fringe96/papers/seymour-cumming/.

Singhroy, V., Mattar, K.E. and Gray, A.L., (1998). Landslide characterisation in Canada using interferometric SAR and combined SAR with TM images. *Advances in Space Research*, Vol.21, No.3, pp.465-476.

Stramondo, S., Tesauro, Briole, P., Sansosti, E., Salvi, S., Lanari, R., Anzidei, M., Baldi, P., Fornaro, G., Avallone, A., Buongiorno, M.F., Franceschetti, G. and Boschi, E, (1999). The September 26, 1997 Colfiorito, Italy, Earthquakes: modeled coseismic curface cisplacement from SAR interferometry and GPS. *Geophysical Research Letters*, Vol. 26, No.7, pp.883-886.

Thiel, K.-H., Wu, X.-Q. and Hartl, P., (1997). ERS-tandem-interferometric observation of volcano activities in Iceland. *The 3rd ERS SYMPOSIUM, Florence, 17 - 21 March 1997.* http://jupiter.esrin.esa.it/pub/florence/papers/data/thiel/index.html

Villasenor, J. and Zebker, H, (1992). Temporal decorrelation in repeat-pass radar interferometry. *IGARSS '92 - 1992 International Geoscience and Remote Sensing Symposium*, Vol.2, pp.941 –943.

Wadge, G, (1997). Volcano monitoring using interferometric SAR. *The 3rd ERS Symposium*, Florence, 17 - 21 March 1997. http://jupiter.esrin.esa.it/pub/florence/papers/.

Wright, P.A. and Stow, R.J., (1997). Detection and measurement of mining subsidence by SAR interferometry. *1997 IEE Colloquium on Radar Interferometry (Digest No.: 1997/153)*, pp. 5/1 -5/6.

Xu, W. and Cumming, I., (1999). A region-growing algorithm for InSAR phase unwrapping. *IEEE Transactions on Geoscience and Remote Sensing*, Vol.37, No.1, pp.124 -134.

Zebaker, H. and Goldstein R., (1986). Topographic mapping from interferometric observations. *Journal of Geophysic Research*, Vol. 91, No. B5, pp.4993-4999.

Zebker, H.A., Madsen, S.N., Martin, J., Wheeler, K.B., Miller, T., Lou, Y., Alberti, G., Vetrella, S. and Cucci, A., (1992). The TOPSAR interferometric radar topographic mapping instrument. *IEEE Transactions on Geoscience and Remote Sensing*, Vol.30, No.5, pp.933 –940.

Zebker, H.A. and Villasenor, J., (1992). Decorrelation in interferometric radar echoes. *IEEE Transactions on Geoscience and Remote Sensing*, Vol.30, No.5, pp.950 –959.

Zebker, H.A. and Rosen, P., (1994). On the derivation of coseismic displacement fields using differential radar intererometry: The Landers earthquake. *IGARSS '94 - 1994 International Geoscience and Remote Sensing Symposium on Surface and Atmospheric Remote Sensing: Technologies, Data Analysis and Interpretation*. Vol.1, pp.286 –288.